Available online at www.sciencedirect.com

SCIENCE DIRECT®

Earth and Planetary Science Letters 224 (2004) 213–228

EPSL

www.elsevier.com/locate/epsl

Evolution of the northern Main Ethiopian rift: birth of a triple junction ☆

Ellen Wolfenden[a], Cynthia Ebinger[a,*], Gezahegn Yirgu[b], Alan Deino[c], Dereje Ayalew[b]

[a] *Department of Geology, Royal Holloway, University of London, Egham, TW20 0EX, UK*
[b] *Department of Geology and Geophysics, Addis Ababa University, PO Box 1176, Addis Ababa, Ethiopia*
[c] *Berkeley Geochronology Center, 2245 Ridge Road, Berkeley, CA, USA*

Received 25 November 2003; received in revised form 28 February 2004; accepted 19 April 2004

Abstract

Models for the formation of the archetypal rift–rift–rift triple junction in the Afar depression have assumed the synchronous development of the Red Sea–Aden–East African rift systems soon after flood basaltic magmatism at 31 Ma, but the timing of intial rifting in the northern sector of the East African rift system had been poorly constrained. The aims of our field, geochronology, and remote sensing studies were to determine the timing and kinematics of rifting in the 3rd arm, the Main Ethiopian rift (MER), near its intersection with the southern Red Sea rift. New structural data and 10 new SCLF $^{40}Ar/^{39}Ar$ dates show that extension in the northern Main Ethiopian rift commenced after 11 Ma, more than 17 My after initial rifting in the southern Red Sea and Gulf of Aden. The triple junction, therefore, could have developed only during the past 11 My, or 20 My after the flood basaltic magmatism. Thus, the flood basaltic magmatism and separation of Arabia from Africa are widely separated in time from the opening of the Main Ethiopian rift, which marks the incipient Nubia–Somalia plate boundary; triple junction formation is not a primary feature of breakup above the Afar mantle plume. The East African rift system appears to have propagated northward from the Mesozoic Anza rift system into the Afar depression to cut across Oligo-Miocene rift structures of the Red Sea and Gulf of Aden, in response to global plate reorganisations. Structural patterns reveal a change from 130°E-directed extension to 105°E-directed extension sometime in the interval 6.6 to 3 Ma, consistent with predictions from global plate kinematic studies. The along-axis propagation of rifting in each of the three arms of the triple junction has led to a NE-migration of the triple junction since 11 Ma.

Keywords: triple junction; rift; Red Sea; Ethiopian rift; flood basalts

1. Introduction

The seismically and volcanically active rift system in Ethiopia is one of the few areas worldwide where one can capture the ongoing process of continental break-up associated with a mantle plume (e.g., [1,2]) (Fig. 1, inset). The Main Ethi-

☆ Supplementary data associated with this article can be found, in the online version, at doi:10.1016/j.epsl.2004.04.022.

* Corresponding author. Tel.: +44-1784-443890; fax: +44-1784-471780.
E-mail address: cindy@gl.rhul.ac.uk (C. Ebinger).

0012-821X/$ - see front matter © 2004 Elsevier B.V. All rights reserved.
doi:10.1016/j.epsl.2004.04.022

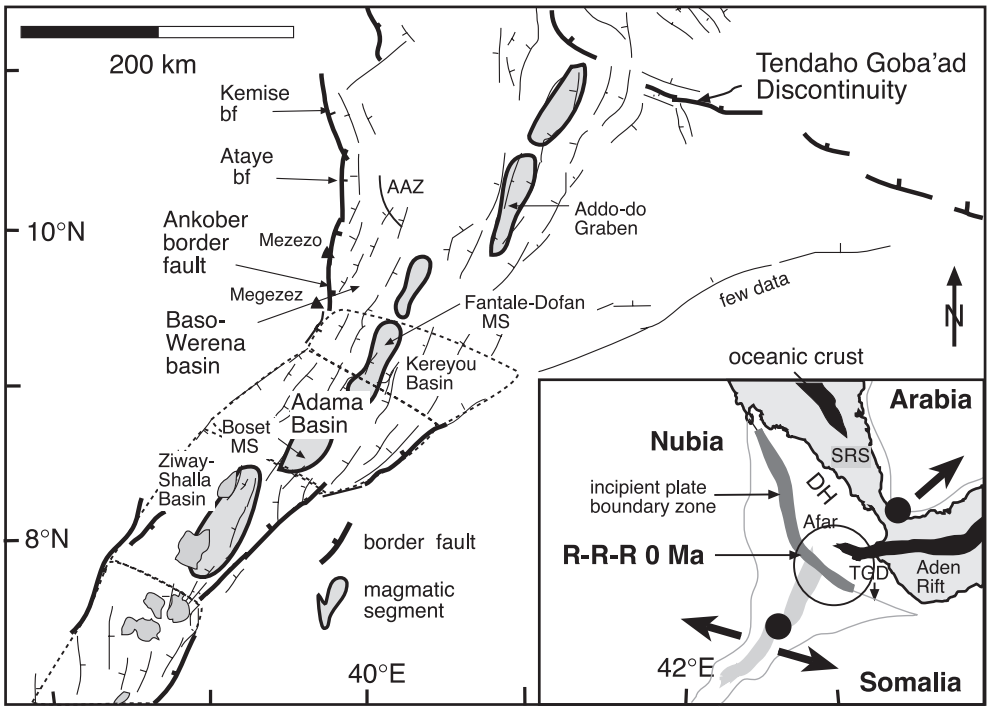

Fig. 1. Major faults and along-axis segmentation patterns within the southern Red Sea and northern Main Ethiopian rift. Inset shows extent of new oceanic crust (black) and present-day southern Red Sea (SRS)–Gulf of Aden–Main Ethiopian rift triple junction zone. Arabia and Africa can be reconstructed crudely by overlying black dots. TGD is Tendaho–Goba'ad discontinuity separating the Red Sea and MER; DH is Danakil horst. Extension directions (bold arrows) from [24,45].

opian and Red Sea rifts also preserve a wealth of information on hominid evolution and early habitats [3]. The Red Sea, Gulf of Aden, and Ethiopian rifts intersect in a complex zone within the central Afar depression, producing the archetypal rift–rift–rift triple junction zone associated with a mantle plume [4]. Although Afar triple junction models have assumed synchronous development of all three rift arms [2,4,5], too few data were available to evaluate the longer term stability of the plate boundaries [6].

Field studies and exploration seismic, gravity, and well data constrain the timing of initial sedimentation and faulting within the Red Sea and Gulf of Aden, but the timing and geometry of initial rifting in the third arm, the Main Ethiopian rift, were only loosely constrained by sparse geochronological data [7,8]. Thus, the development of the Red Sea and Ethiopian rift intersection is the 'missing piece' in our understanding of triple junction formation and continental break-up in the Afar depression.

This project aims to determine the timing of development of the Ethiopian rift and its implications for the evolution of the Red Sea–Gulf of Aden–Main Ethiopian triple junction. Field, remote sensing, and geochronology studies were undertaken in the deeply incised volcano-sedimentary section lying in the intersection between N–S trending Red Sea rift faults, and NE-trending Ethiopian rift faults (Figs. 1 and 2). Our specific objectives were to establish a tectono-stratigraphic framework for the northern Main Ethiopian rift by (1) logging stratigraphic sequences above and below an angular unconformity exposed in the >500-m-deep Kessem river gorge; (2) collecting and analyzing volcanic and volcaniclastic rock samples using high precision single-crystal laser fusion techniques; (3) using remote sensing imagery to map stratigraphic units and faults throughout the northern Main Ethiopian

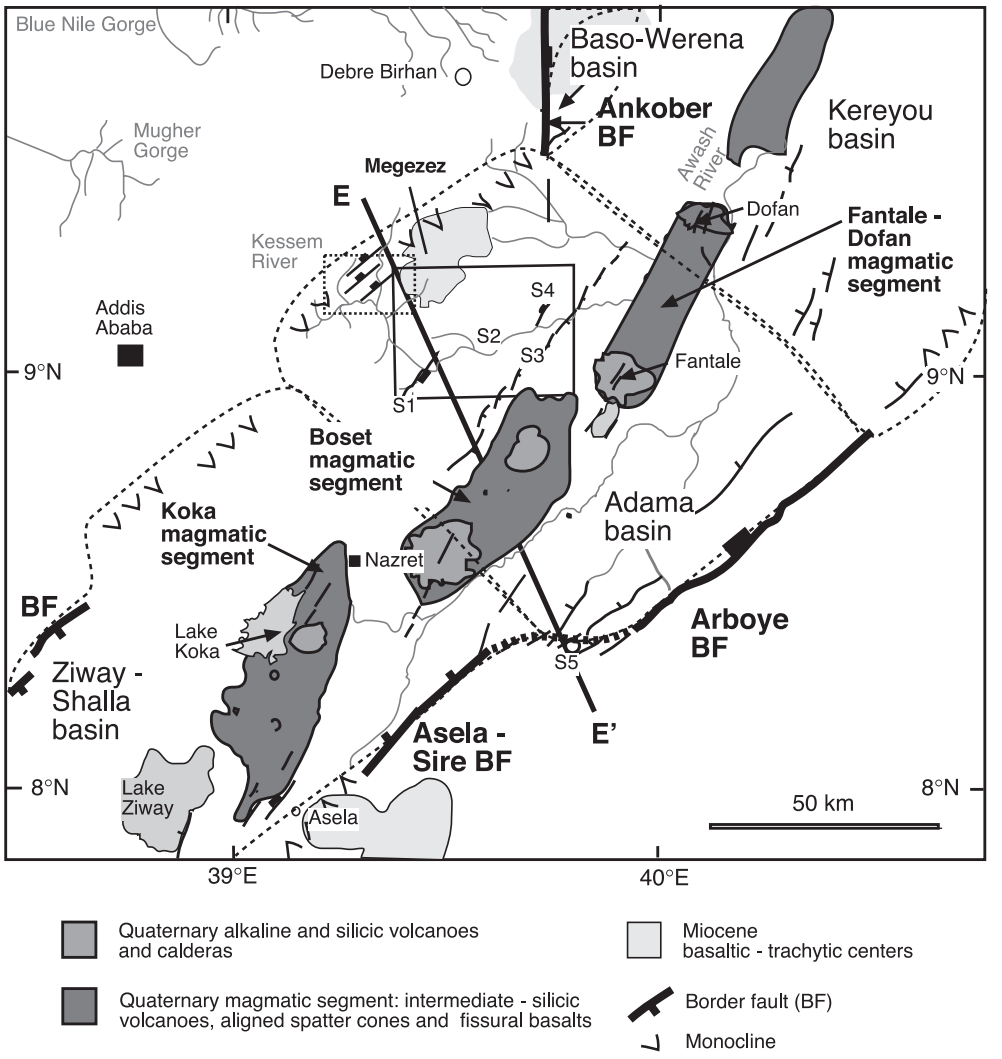

Fig. 2. Summary tectonic map of study area. Dashed box encloses area shown in Fig. 6, bold box encloses area shown in Fig. 7. Cross-section E–E′ in Fig. 3. S1–S5 are field sample locales (Table 1).

rift (MER). We integrate these results with those of ongoing work to establish a tectono-stratigraphic history for the Afar depression.

2. Tectonic setting

The Red Sea–Aden–Main Ethiopian rift–rift–rift triple junction lies on the broad Ethiopian plateau, believed to have developed above a Palaeogene mantle plume [9,10]. Compilations of $^{40}Ar/^{39}Ar$ data from the Red Sea and Gulf of Aden regions show that flood basalts and associated felsic rocks were erupted across a ~1000 km diameter region between 31 and 29 Ma [11–13], roughly coeval with the initiation of NE-directed extension in the southern Red Sea [14], and the Gulf of Aden [15] (Fig. 1). Initial rifting in the southern and central Main Ethiopian rift (MER) commenced between 18 and 15 Ma, but little was known of rift initiation in the northern MER [7,16]. Northeast-directed seafloor spreading in the Gulf of Aden has propagated

westward into the Afar depression since 16 Ma [17]; northeast-directed seafloor spreading in the Red Sea commenced at ca. 4 Ma [18]. Seafloor spreading has yet to begin in the MER.

The present-day Red Sea–Gulf of Aden–Main Ethiopian rift triple junction lies in a complex zone at ~11.5°N within the central Afar depression [19,20] (Fig. 1). The evolution of the triple junction, however, is controversial owing to poor constraints on the kinematics of Nubia (stable Africa)–Somalia–Arabia plate motions [6,21]. One class of models shows Arabia and a narrow sliver of the Nubian plate, the Danakil plate, rotating counter-clockwise about a pole in the Red Sea region [22,23]. These models predict pure strike-slip deformation and counter-clockwise rotations in the northern Main Ethiopian rift at ~31 Ma, which are opposite to the rotations measured by Acton et al. [19]. In an alternative approach, Eagles et al. [6] use poles of rotation determined from global plate motions studies, and show oblique-slip motion throughout the southern Red Sea and northwestern Afar depression. This model does not require any differential movement between Nubia and Somalia until after 12 Ma [6]. Tesfaye et al. [5] interpret an arcuate pattern of faults seen in high resolution imagery as an accommodation zone marking an Oligocene triple junction at ca 10°N latitude, which then migrated northeastward to its present location (Fig. 1). They could, however, only infer the age of these structures.

Prior to this study, there were few constraints on the timing of rift initiation in the northernmost MER where the rift broadens into the structurally complex Afar depression. Chernet et al. [8] sampled sequences throughout the northern MER and suggested that rifting commenced at ~7 Ma, based on the onset of bimodal basalt–rhyolite volcanism. They noted a phase of widespread, predominantly basaltic magmatism at ~10 Ma [8]. Geodetic data show that present-day extension within the northern Main Ethiopian rift has localised to <20 km-wide zones of aligned volcanoes and associated flows [24]. These Quaternary 'magmatic segments' developed after 1.8

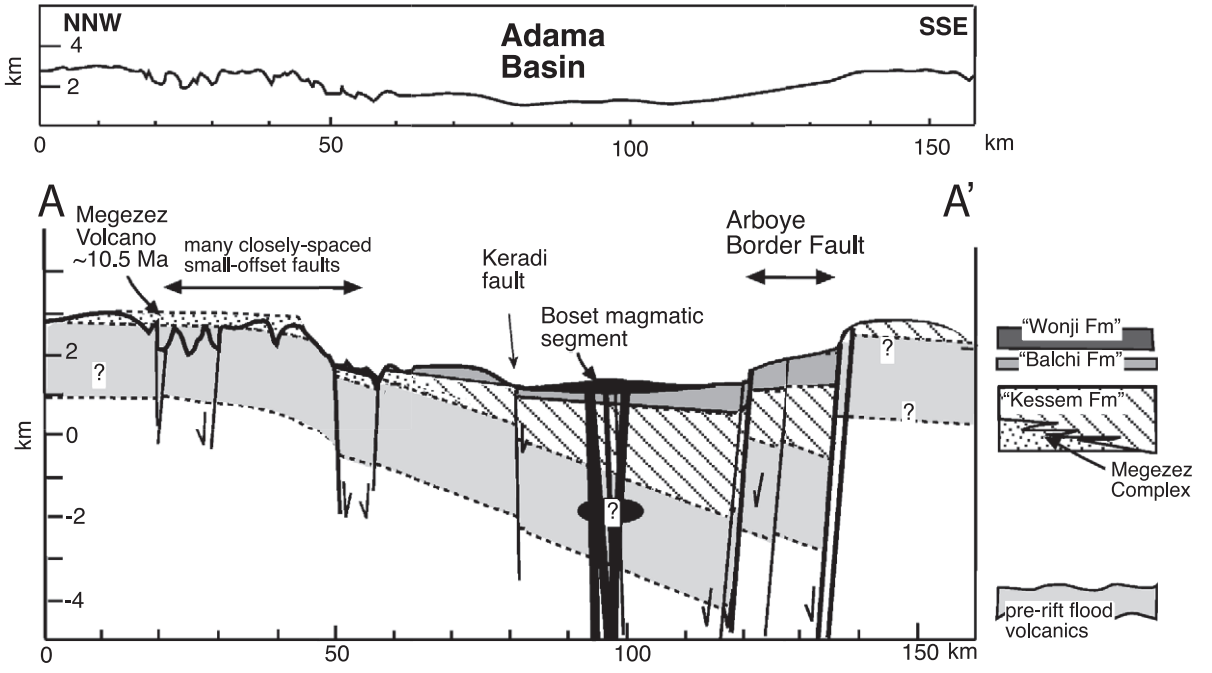

Fig. 3. Topography (top) and cross-section of the Adama basin along line E–E′ (Fig. 2), showing half-graben form of the basin and onlapping patterns along the NW side of the basin. These patterns are typical of rift basins throughout E Africa. Note narrow zone of dyke injection and faulting near the center of the basin.

Ma; they are cut by en echelon fault zones and fissures [25,26]. The Quaternary magmatic segments of the MER are superposed on the older Red Sea and Aden rift structures in the Afar depression [1,14] (Fig. 1).

Our work focuses on the development of the Adama basin of the Main Ethiopian rift, and its tectonic relationship to the southernmost Red Sea rift (Figs. 1 and 2). The northern termination of the basin is the Ankober border fault, which developed during or immediately after the emplacement of Mezezo volcano at ~11 Ma [13] (Fig. 1). The general form of the Adama basin is illustrated in a summary cross-section made from new and existing data (Fig. 3). We have simply projected stratal dips beneath the basin, providing a crude depth estimate of ~4 km, which is consistent with the 3.5-km-depth estimated from preliminary results of seismic refraction studies in the rift [27]. The Adama basin is asymmetric and tilted to the southeast toward the large offset normal faults bounding the southeastern basin margin (Arboye border fault system). These faults form a staircase pattern rising to the ~2600-m level of the uplifted rift flanks. The NW side of the basin is a faulted flexure (Fig. 2). Models of gravity and geodetic data suggest that the narrow magmatic segments are underlain by mafic intrusives [24,28] interpreted by Ebinger and Casey [26] as a zone of intensive dyke injection.

3. Stratigraphy

Existing geochronological data for the northern Main Ethiopian rift are sparse and of variable quality. Except for the work of Ukstins et al. [13], available details of sample locales from previous studies are too imprecise to compare with our local stratigraphies.

3.1. Radiometric age determinations

Samples of volcaniclastic and basaltic units were collected along transects of the deeply incised northwestern margin of the Adama basin for petrographic analyses and radiometric age determinations (Fig. 2). Thin sections of volcanic samples were examined for alteration, and only samples with fresh, but sometimes cracked, feldspars were analyzed using single-crystal laser fusion methods (Appendix A).

All feldspar samples yielded individual-grain age distributions that were strongly dominated by a single peak, interpreted to represent the time of eruption. A few outliers (2σ beyond the mean) and two grains with anomalously low radiogenic ^{40}Ar content (<80%) were omitted from further data analysis. A summary of the single-crystal, total-fusion analytical results is given in Table 1, and full data tables are provided in the on-line archive (Table Archive1).

The single incremental-heating experiment performed on HF-treated basalt groundmass of sample E01-10 yielded the spectrum shown in Fig. 4. The release pattern exhibits a plateau across almost the entire experiment, with an age of 3.47 ± 0.04 Ma. (By comparison, a control experiment not shown on the same groundmass, but without HF treatment, yielded a highly discordant, stair-step downward pattern.) An 'inverse' $^{36}Ar/^{40}Ar$ vs. $^{39}Ar/^{40}Ar$ isochron analysis of the HF-treated experiment yielded a nearly identical age of 3.49 ± 0.04 Ma, with a 'trapped' $^{40}Ar/^{36}Ar$ intercept of 294.5 ± 1.9 (MSWD = 0.7). The age derived from the isochron is taken as the reference age for this sample.

Below we subdivide the Neogene–Recent sequences within the northernmost Main Ethiopian rift according to tectonic situation within the basin. Data from the Adama basin include the single-crystal laser fusion (SCLF) $^{40}Ar/^{39}Ar$ dates of sanidine separates from two units in the Kessem gorge [13].

3.2. Pre-rift sequences

Deeply incised gorges cut into the uplifted flanks of the Adama basin expose Pan-African metamorphic basement and marine sedimentary strata deposited on a passive continental margin in Mesozoic time [32,33]. Overlying the Mesozoic sequences are Oligocene–Lower Miocene flood basalts (Fig. 3). George [33] used the whole rock $^{40}Ar/^{39}Ar$ dating method and Chernet et al. [8] used K–Ar methods to date basalts overlying Mesozoic strata on the northeastern basin margin at 26 to 23.4 Ma, narrowing the range of values obtained in earlier K–Ar studies [34,35]. Chernet et al. [8] provide 23.8–24.1 Ma K–Ar dates of basalts overlying Mesozoic strata on the southeastern margin range, within the range of earlier values (22 to 28 Ma [36]).

Table 1
Latitude and longitude of rock samples indicated below sample number

$^{40}Ar^*/^{39}Ar$ Single-Crystal Dating Results												
Sample	Lon	Lat	Lab ID #	$J\pm1\sigma$ ($\times10^3$)		n/n_0	MSWD	Ca/K$\pm1\sigma$		$^{40}Ar^*/^{36}Ar\pm1\sigma$		Age$\pm1\sigma$	
Sanidine													
E01-14A	39.5501	9	22345	5.159	0.005	11/13	1.4	0.0037	0.0000	0.3800	0.0006	3.555	0.007
E01-17	39.5764	9.05	22485	0.6586	0.0006	19/23	2.5	0.0001	0.0002	2.6095	0.0022	3.098	0.009
E01-18	39.5675	9.03	22486	0.6585	0.0006	18/20	0.9	0.0142	0.0004	8.5624	0.0060	10.144	0.012
E01-26	39.6325	9	22354	5.210	0.005	13/15	2.5	0.0095	0.0001	0.2706	0.0006	2.540	0.018
E01-40	39.5428	9.18	22351	5.195	0.005	13/14	0.7	0.0030	0.0000	0.7075	0.0007	6.619	0.009
E01-41	39.7218	9.16	22347	5.178	0.005	12/14	1.0	0.1316	0.0003	0.7708	0.0009	7.186	0.011
E01-42	39.7253	9.14	22353	5.206	0.005	5/5	1.2	0.0110	0.0001	1.0687	0.00164	10.008	0.018
HS-01	39.6729	8.34	22344	5.177	0.005	15/16	0.6	0.0133	0.0001	0.8377	0.0009	7.807	0.011
HS-02	39.6699	8.35	22348	5.181	0.005	14/14	2.0	0.0022	0.0000	0.8554	0.0009	7.98	0.03
Plagioclase													
E01-3A	39.5653	9.04	22350	5.190	0.005	7/8	1.2	8.7223	0.0275	0.1313	0.0051	10.56	0.05

Notes: Stated uncertainty in weighted mean includes error in J, the neutron fluence parameter. Ca/K is calculated from $^{37}Ar/^{39}Ar$ using a multiplier of 1.96. 'n/n_0' is the number of individual grain analyses accepted for calculation of the weighted-mean sample age, over the total number of analyses performed. 'MSWD' if the mean sum of weighted deviates of the individual ages. $^{40}Ar^*/^{39}Ar$ is the ratio of radiogenic argon from the decay of ^{40}K to ^{39}Ar derived from irradiation of ^{39}K in the sample. $\%^{40}Ar^*$ is the percentage of radiogenic argon in the total measured ^{40}Ar. $\lambda=5.543\times10^{-10}y^{-1}$. Isotopic interferences resulting from irradiation of Ca in the sample: $(^{36}Ar/^{37}Ar)_{Ca}=(2.72\pm0.01)\times10^{-4}$, $(^{39}Ar/^{37}Ar)_{Ca}=(6.7\pm0.4)\times10^{-4}$. Isotopic interference resulting from irradiation of K in the sample: $(^{40}Ar/^{37}Ar)_K=(7\pm3)\times10^{-4}$.

3.3. Southeastern margin

Morbidelli et al. [36] analyzed two samples from along the southeastern rift flank. These were dated using K–Ar methods at 12.6 Ma (whole rock) and 11.7 Ma (feldspar separates). Chernet et al. [8] used K–Ar method to determine an age of 10.3 ± 0.2 Ma for a basalt from the lowest of several scarps forming the Arboye border fault. Two conformable ignimbrites exposed along the easternmost fault of the Arboye border fault system were sampled for dating in the hopes that this fault would expose older strata (J. Rowland, personal communication, 2001). Samples HS02 and HS01 collected from the same stratigraphic package were dated at 7.98 ± 0.05 and 7.807 ± 0.011 Ma, respectively (Table 1). These units were originally mapped by Berhe and Kazmin [32] as the Mid-Miocene to Pliocene Nazret Group, which we subdivide below.

3.4. Northwestern margin

Trachytic flows commonly containing lathe-like feldspar phenocrysts that emanated from Megezez volcano overlie the flood basalts on the flexural margin of the Adama basin. Trachyte flows from the base of Megezez were dated at 10.5 ± 0.2 Ma (whole-rock $^{40}Ar/^{39}Ar$ [33]) and 10.4 ± 0.2 Ma (K–Ar [8]), narrowing the range of 13–11 Ma from previous K–Ar studies [34]. The hiatus between top flood basalts and conformable felsic lavas is consistent with the hiatus recorded on the southeastern rift margin. We see no evidence for deep dissection or laterite formation at the top of the flood basalts, which dip 5–10°SE.

Exposure along a new road cut into the southern flank of Megezez reveals basalts onlapping inferred Megezez flows. The contact could be inferred from colour and textural patterns in ground-truthed imagery across the field areas (supplementary material: see the online version of this article for Figs. D1–D3). The stratigraphically lowest sequences in the Kessem gorge and the most heavily dissected are fine-grained basalts and intercalated ignimbrites (Fig. 5). Sample E01-3a was dated at 10.56 ± 0.05 Ma, identical to a date of 10.58 ± 0.07 Ma from strata on a nearby fault block [13]. The lowermost stratigraphic sequence includes thin fluvial sequences of reworked tuffs and

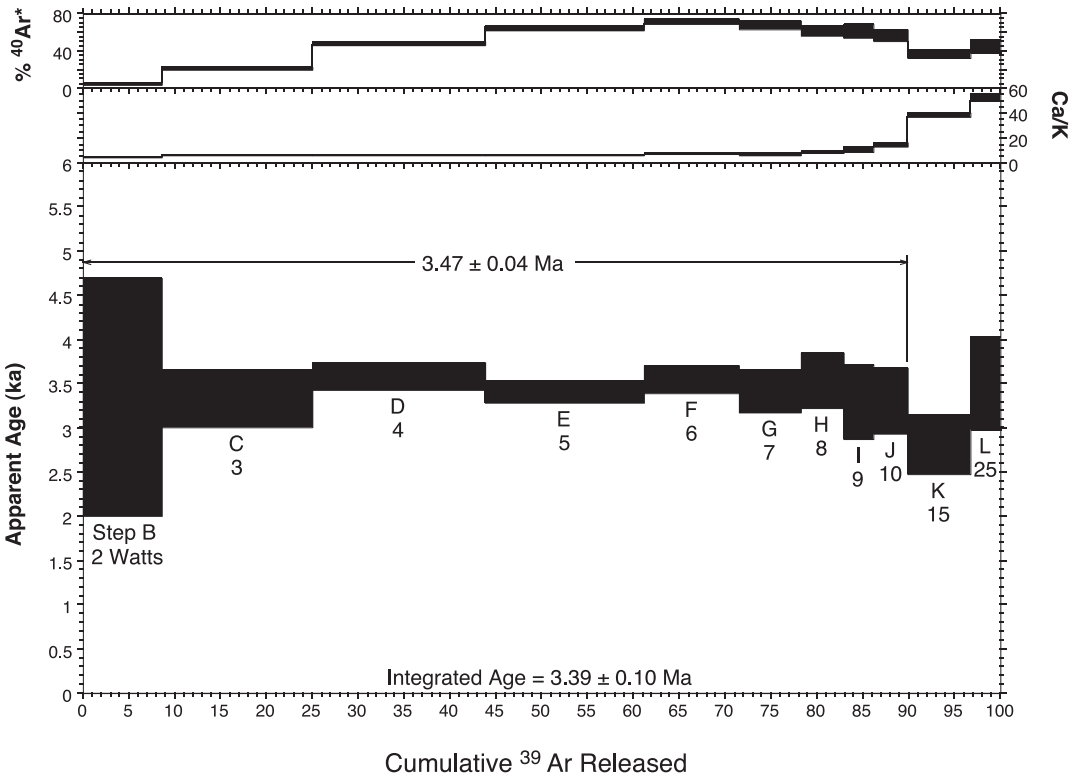

Fig. 4. The single incremental-heating experiment performed on HF-treated basalt groundmass for sample E01-10 (see Data Archive). The release pattern exhibits a plateau across almost the entire experiment, with an age of 3.47 ± 0.04 Ma. By comparison, a control experiment not shown on the same groundmass, but without HF treatment, yielded a highly discordant, stair-step downward pattern. An 'inverse' $^{36}Ar/^{40}Ar$ vs. $^{39}Ar/^{40}Ar$ isochron analysis of the HF-treated experiment yielded a nearly identical age of 3.49 ± 0.04 Ma, with a 'trapped' $^{40}Ar/^{36}Ar$ intercept of 294.5 ± 1.9 (MSWD = 0.7).

some baked soil horizons. An ignimbrite (E01-18) dated at 10.144 ± 0.012 Ma comes from near the top of this package of tilted volcanic units, which we refer to as the Kessem formation (Fig. 5).

The Meteh Bila field locality shows similar relations to the Kessem formation in the Kessem gorge, but with considerable differences in thickness and duration. The stratigraphically lowest unit sampled was an ignimbrite from a thick sequence of felsic lavas overlying a further 250 m or more of altered basalts and felsic lavas. This stratigraphic package showed multiple unconformities. Sample E01-42 was dated at 10.008 ± 0.018 Ma, stratigraphically linking the felsic units above the altered basalts with the Kessem formation. A feldspar-rich tuff (E01-41) near the top of the sequence was dated at 7.186 ± 0.011 Ma. The topmost ignimbrite unit, E01-40, was dated at 6.619 ± 0.009 Ma; it forms widespread mesas at ~ 1600-m elevation, and marks the top of the synrift sequences in the area. Two other flows within this area were dated using K–Ar methods by Chernet et al. [8] at 5.8 ± 0.3 and 6.8 ± 0.2 Ma, but their sample locales are too imprecise to compare his ages to particular units within our stratigraphy. Scoria cones overlie the widespread ignimbrite near Meteh Bila.

In the Kessem gorge localities, an erosional unconformity separates the steeply tilted lower units (25–35°SE) from strata dipping < 15°SE at the top. This unconformity is channelised and overlain by a volcanic-boulder conglomerate that is very similar to the present-day Kessem river bed deposits. Ukstins et al. [13] dated an ignimbrite < 10 m above the ancient river bed deposits at 3.19 ± 0.04 Ma (Fig. 5). A basalt

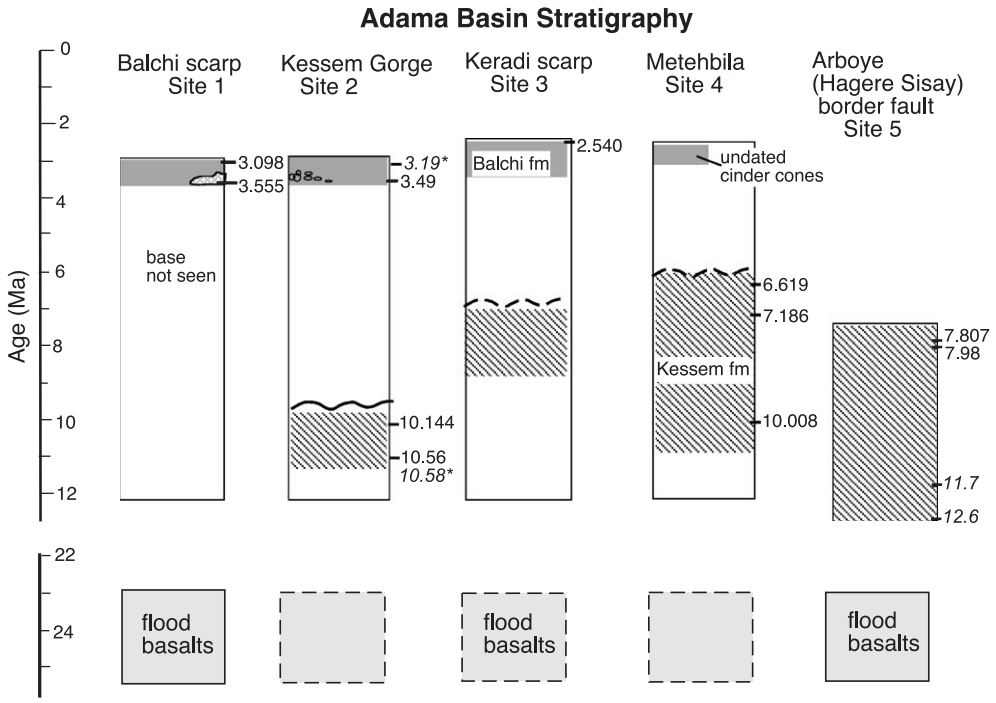

Fig. 5. Summary stratigraphic columns for the 5 field locales shown in Fig. 2. Ages in bold from this study (Table 1); bold italicised Ar–Ar dates from Ukstins et al. [13]; italicised K–Ar dates of mineral separates from Morbidelli et al. [34] Constraints on age of pre-rift flood basalts are Ar–Ar dates in George [32]. (Detailed stratigraphic columns from the field locales available upon request.)

from the base of the sequences above the unconformity on the north side of the Kessem river, E01-10, was dated at 3.49 ± 0.04 Ma. Considering the incision by the palaeo-Kessem river, sample E01-10 suggests that the unconformity spans the period 6.6–3.5 Ma.

Volcanic strata sampled from a fault scarp topographically higher up the escarpment than the Kessem gorge provide constraints on the timing of faulting in the region. Rhyolitic intrusives and extrusive block and ash units, interpreted as collapsed domes, mark and are cut by the Balchi fault (Fig. 2). One of these rhyolitic centers was dated at 3.555 ± 0.007 Ma (E01-14A, Table 1). Overlying units are conformable and dip <15°SE, with the topmost ignimbrite dated at 3.098 ± 0.009 Ma (E01-17, Table 1).

We also dated strata from topographically lower, but structurally similar sequences to the east of the Kessem river localities. A thin ignimbrite (E01-26) within a predominantly basaltic sequence exposed along the NE-striking Keradi fault system was dated at 2.540 ± 0.018 Ma (Table 1, Fig. 7). We correlate these felsic and mafic sequences with the Balchi formation. An unfaulted lahar and intercalated ignimbrite infills the lower Kessem gorge south of Meteh Bila and west of the Kessem fault, attesting to more recent volcanic activity.

3.5. Central Adama basin

Plio-Pleistocene volcanic, volcaniclastic, and minor lacustrine strata overlie the Pliocene Balchi Formation within the central Adama basin [8,32]. Very few of the units have been dated with K–Ar methods, and so lateral correlations varied from author to author (see [8] for review). Chernet et al. [8] show that units on or near the Wonji fault zone were erupted after 1.6 Ma. Boset and Fantale volcanoes and smaller aligned eruptive centres were constructed since ~1.8 Ma, and eruptive products are both felsic and basaltic [8,25] (Fig. 2). This tectono-stratigraphic unit is referred to as the Wonji Group [32].

4. Structure

Remote sensing data were used to map dated stratigraphic sequences throughout the study region, and to extend fault interpretations across a broader region. Landsat-7 Thematic Mapper imagery (15- and 30-m resolution) provide a regional context and allow us to infill gaps between traverses and across numerous faults. Reconnaissance work on the southeastern margin of the rift provided a framework for interpretation of the Adama basin (e.g., Figs. 2, 6 and 7).

Exposures in the deeply incised canyons of the NW rift margin, as well as rivers flowing SE away from the uplifted Arboye border fault flank provide a nearly 3D picture of the flood volcanic sequences (e.g., Fig. 6). Flat-lying flood volcanic sequences are tilted ~ 5°SE along a broad monocline, and are covered by distal ignimbrite and tuff pairs. The undated felsic strata thicken eastward toward Megezez volcano, and are probably products of the ~ 11 Ma eruptions at Megezez and/or Mezezo volcano (Fig. 1). Important to note is the absence of an incised erosional surface at the top of the flood volcanic sequences, arguing against local fault-controlled topography (Fig. 6). The Oligocene lavas show no thickening into faults, which clearly post-date their emplacement (e.g., Fig. 6). Oligocene volcanic sequences exposed on the SE rift flank also show parallel bedding [36]. Thus, we infer that development of the MER post-dates the emplacement of the flood volcanic sequences.

A detailed cross-section of the northwestern Adama basin margin illustrates the key structural and stratigraphic relations used to determine the timing of rift basin development (Figs. 7 and 8). Section B–B′ (Fig. 8) links field locales in the Kessem gorge area but is slightly oblique to major faults. Stratal tilts within the

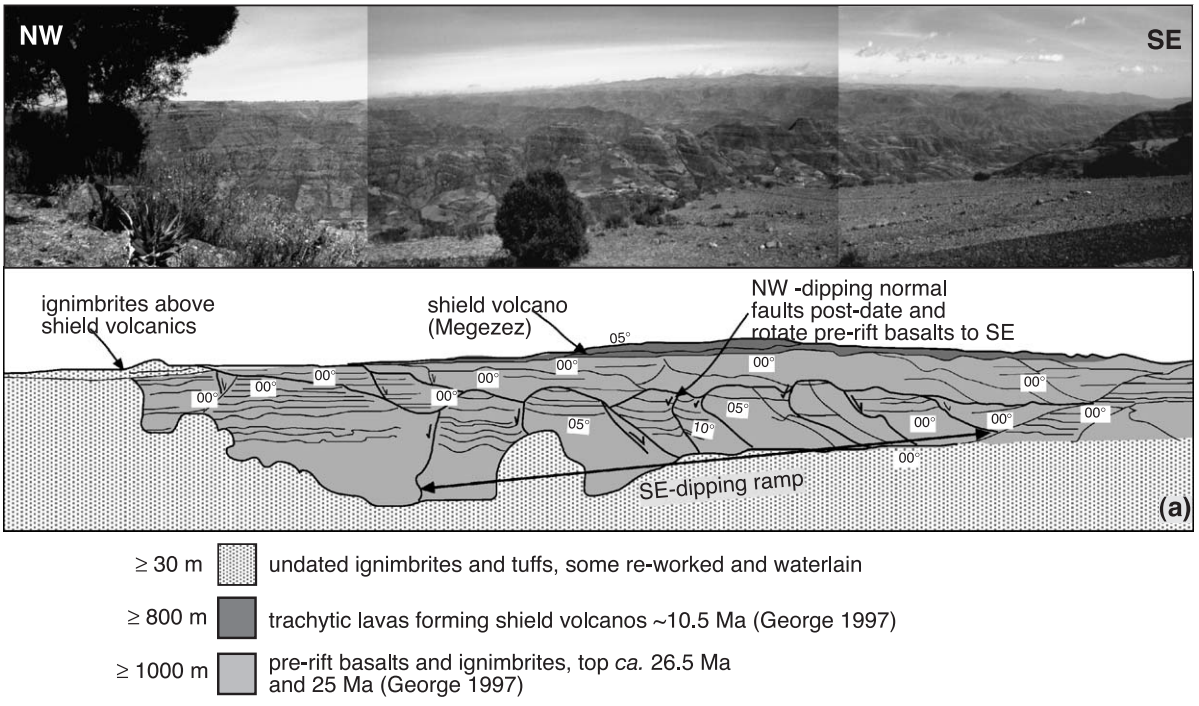

Fig. 6. Photo montage and line drawing illustrating structural setting of Oligocene flood volcanic strata and overlying syn-rift strata along the NW basin margin (Fig. 2). Top: Photo looks east toward Megezez volcano across the 3D exposures of the upper Kessem river, which exposes 1200 m of basalts and intercalated ignimbrites. Dates from George [33]. The upper Miocene strata are conformable, with no evidence for faulting or extensive erosion during the intervening period (~ 24 to ~ 11 Ma). The pre-rift flood volcanics and syn-rift units show a regional SE dip. The contact between Megezez and flood volcanics can be traced in imagery throughout the region (Data repository).

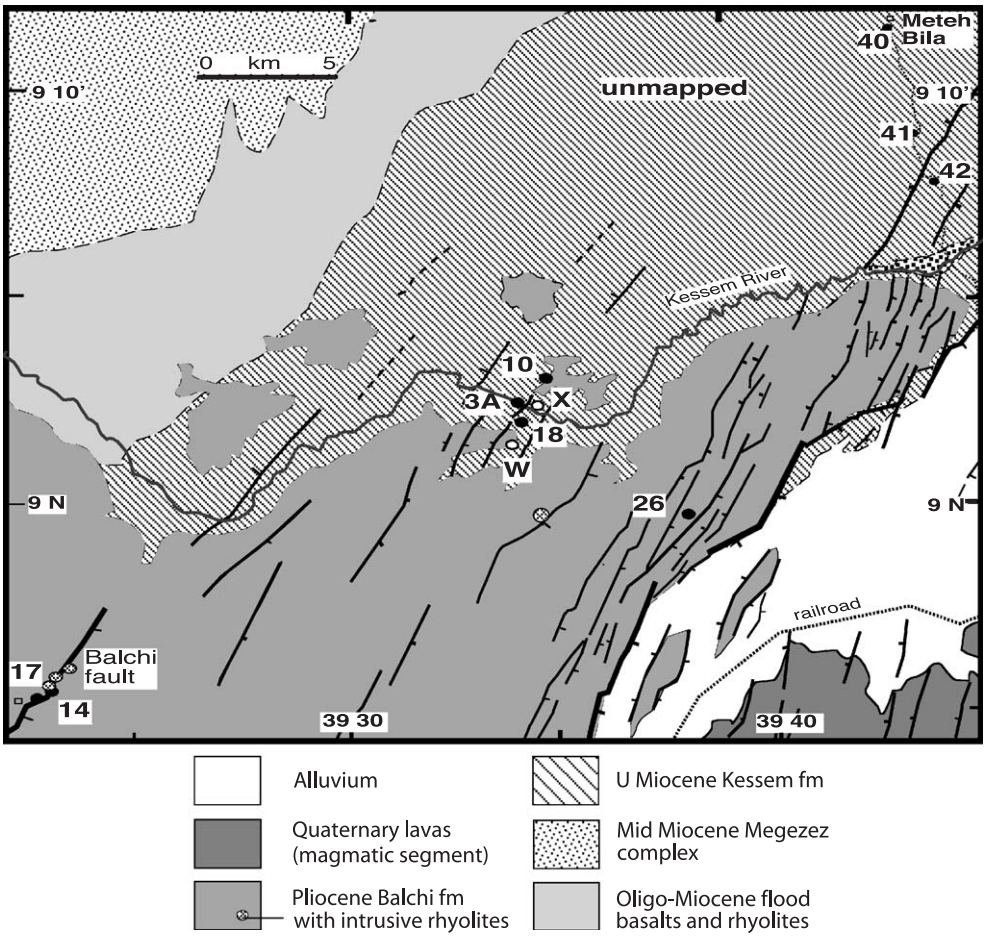

Fig. 7. Structural interpretation of field observations extended to a wider zone using enhanced high-resolution Landsat-7 imagery. Fault widths proportional to throw, but total throw on Keradi fault not shown to enable display of unconformity. Cross-section B–B′ is shown in Fig. 8. Locations of dated samples shown (Table 1). W, X are samples collected by EW, with dates presented by Ukstins et al. [13].

Kessem formation are 25–35°SE, and volcaniclastic units thicken toward N35–45°E-striking normal faults. The overlying Balchi formation is cut by fewer faults showing a N10–20°E strike, which is consistent with the orientation of faults and fissures within the Pleistocene Wonji formation (e.g., Fig. 7).

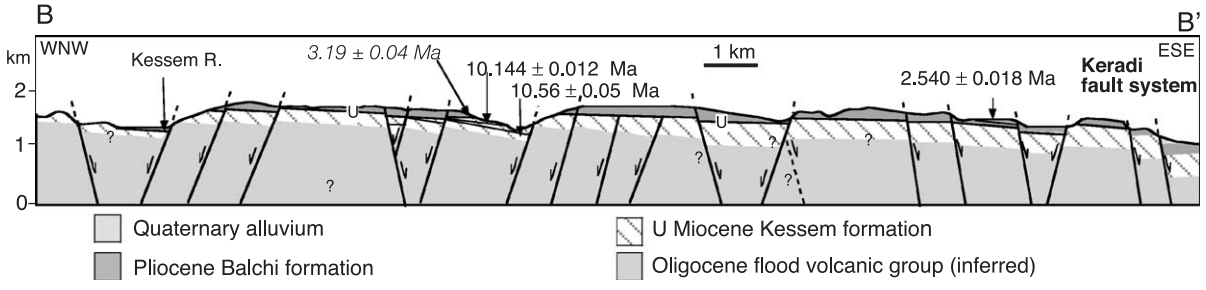

Fig. 8. Cross-section B–B′ (Fig. 7) across the NW margin of the Adama basin. Dates from this study (Table 1).

Volcanic and volcaniclastic sequences within the structurally complex 'corner' between the NE-trending MER and the N–S trending Red Sea rift show much greater strains than any other field locality in the northern MER, as well as the southern Red Sea rift [14] (Figs. 2 and 7). Faults are closely spaced, and throws are more than 500 m along segments of the Keradi fault system, which exposes the unconformity (Figs. 2 and 7). The Kessem formation is rotated ~ 35° into one or more steeply dipping monoclinal folds. Post-2.5 My movement along the Keradi fault system, which intersects N10°E-striking faults parallel to the Ankober border fault, forms a complex linkage zone between the southern Red Sea and Main Ethiopian rift (Figs. 2 and 7). The uppermost Kessem sequences near Meteh Bila, however, comprise thick packages of ash and pumice, indicating a nearby eruptive source. Hence, the longer time interval and thicker preserved sequence may be a consequence of proximity to volcanic sources and creation of synrift accommodation space around a high strain zone.

5. Adama basin evolution

Structural and stratigraphic relationships within the Adama basin and surrounding regions indicate that the northernmost Main Ethiopian rift developed during or soon after the emplacement of Megezez volcano at ca. 10.6 Ma, ~ 18 My after initial rifting in the southern Red Sea and Gulf of Aden [14]. The hiatus in volcanism between ~ 24 and 10.6 Ma and the lack of incision into the volcanic sequences suggests that this was a period of tectonic quiescence, corresponding to a period of erosion on the Ethiopian plateau to the north [37]. The Kessem formation, which shows growth and syn-sedimentary faulting, onlaps flows from Megezez volcano, based on field and remote sensing data. The Kessem sequence throughout the study area shows a regional southeastward dip, indicating that the broad southeastward basinal tilt developed early in the basin history. Faults that terminate within or at the top of the Kessem formation strike N35–45°E, subparallel to the Arboye border fault. Thus, new and existing data indicate that the Arboye border fault system developed at ~ 10.6 Ma, and it controlled basin geometry during the initial stages of Adama basin formation. Large offsets accumulated along the border fault system after 7.8 Ma, displacing the dated ignimbrites. Clearly, the northernmost MER could have experienced some extensional or transtensional deformation prior to 11 Ma, but the volcanic hiatus, stratigraphic relations from the rift margins, and morphological patterns demonstrate that any pre-11 Ma deformation was minor, and that the northern MER formed after 11 Ma.

The rock record between 6.6 and 3.5 Ma is not exposed along the northwestern basin margin. Between ~ 3.5 and 3.1 Ma, volcanism recommenced within the Adama basin where felsic and basaltic lava flows accumulated above the unconformity. Faults cutting the Balchi formation strike ~ N15°E, whereas faults terminating in the Kessem formation strike ~ N35°E. The Balchi fault comprises several fault segments striking N15°E linked by N35°E-striking faults, suggesting that 10.6–6.5 My faults were preferentially reactivated as transfer faults during subsequent rifting episodes (Fig. 7). Possibly during, and certainly after, the emplacement of the Balchi formation, a long, discontinuous fault system comprising N15°E and N35°E-striking fault segments developed basinward of the Balchi fault. This period of predominantly felsic volcanism is coeval with the emplacement of felsic volcanoes along the central MER margins [7,8], and synchronous with the massive outpouring of lavas in southern Afar (Stratoid series). The renewed, predominantly felsic activity between 3.5 and 2.5 Ma infilled a narrower area of the subsiding basins, producing an offlapping stratigraphic pattern on the flexural margin (e.g., Fig. 3).

Since 1.8 Ma, magmatism and faulting focussed into discrete, en echelon Boset and Dofan-Fantale magmatic segments, which cross-cut the original Adama and Kereyou basin limits (Fig. 1). These patterns demonstrate an episodic narrowing of the zone of active extension, magmatism, and subsidence, as well as changing plate kinematic settings.

6. Plate kinematic implications

Structural and stratigraphic relations in the 10.6 – 6.6 Ma Kessem formation indicate that the N40°E-striking Arboye border fault controlled initial subsidence within the Adama basin, with no syn-rift volcano-sedimentary sequences older than ~ 10.6 My. The conformable contact between Megezez flows/Kessem

formation and the flood basalt sequences argues against significant deformation in the northern MER prior to 10.6 Ma (e.g., Fig. 6). Nowhere in the study region did we find evidence for strike-slip deformation along NE-striking fault systems, as predicted in crank-arm type models for the synchronous opening of the Red Sea, Aden, and Main Ethiopian rifts. We also find no evidence for NW-striking strike-slip fault zones as predicted in the arcuate accommodation zone model of Tesfaye et al. [5]. Thus, our studies argue against the development of a triple junction in the Afar depression before ~ 11 Ma when felsic shields (e.g., Megezez, Mezezo) developed along developing Arboye and Ankober border fault systems (e.g., Fig. 9). Instead, our work and that of Wolfenden et al. [14] show that the southern Red Sea existed as far south as 10°N at 27 Ma, suggesting that the arcuate accommodation zone of Tesfaye et al. [5] (AAZ, Fig. 9) marks the southern termination of the Oligocene Red Sea rift.

These new timing constraints indicate that the NE-directed separation of Africa and Arabia and the onset of E–W extension between the Nubian and Somalian plates are separate events, as predicted by analogue models of oblique convergence between Africa and Eurasia [38]. Bellahsen et al. [38] can explain the geometry of the Arabian plate and its kinematics if they include a broad lithospheric weak zone beneath NE Africa corresponding to the Afar plume. The asymmetric subduction of the Tethys rotates Arabia away from Africa, but there is no opening across the third arm, the MER. Thus, the ~ 31 Ma flood basaltic magmatism appears intimately linked to the separation of Africa and Arabia; its role in East African rifting remains unclear.

Between 12 and 10 Ma, the Ankober border fault formed as the MER propagated NE (Arboye border fault) to effectively link the southern Red Sea and the Main Ethiopian rifts, forming a triple junction for the first time (Fig. 9C). Thus, the flood basaltic magmatism and separation of Arabia from Africa are widely separated in time from the opening of the Main Ethiopian rift arm of the East African rift system. Between 12 and 10 Ma, the southern Red Sea margin propagated southward via the Ankober border fault as the MER propagated NE via the Arboye border fault, effectively linking the southern Red Sea and the Main Ethiopian rifts, forming a triple junction for the first time (Fig. 9C).

Field and remote sensing data indicate that initial crustal extension within the northernmost Main Ethiopian rift began long after initial faulting in the southern and central MER at ~ 18 Ma [7,16]. Placed within the context of rifting throughout East Africa, these new data suggest that the MER propagated north from the ~ 25 My Turkana rift region after ~ 18 Ma, just as the Eastern, or Kenya rift, propagated south from Turkana after 25 Ma [16,39]. The Turkana region overlies lithosphere rifted during Mesozoic time, and it appears to have been a pre-existing lithospheric weak spot [10,16]. The kink in the MER at ~ 8.5°N corresponds to the highest elevation along the length of the MER, and a major drainage divide between the Red Sea and the Turkana depression to the south. Prior to extension at ~ 10 Ma, the MER would have been a geographic barrier to drainage and faunal migration between the East African rift to the south, and the Red Sea–Gulf of Aden regions to the north in Afar.

The MER is clearly the least evolved of the three triple junction arms, but our new data show that it is also ~ 18 My younger than the Red Sea and Aden rifts. Our new age for the initiation of the MER, whose central rift has been stretched to 2/3 its original thickness [26,27], leads to higher time-averaged extensional velocities. If we assume that the ~ 84-km-wide rift valley was originally 56 km wide, then the average extensional velocity for the past 11 My is 2.5 mm/year, or, roughly half the geodetically determined present-day extensional velocity of 4.5 ± 1 mm/year [24]. These estimates are consistent, considering that Buck et al. [40] predict an increase in extensional velocity with time within magmatic rifts as dyke injection processes become more efficient at accommodating strain.

The predominantly N35–45°E faults active during the accumulation of the Kessem formation are superceded by N15°E-striking faults during and after the Balchi formation was erupted, suggesting a change in extension direction after ~ 3 Ma. Assuming that the extension direction is orthogonal to fault strike, the post-3 Ma 105°E extension direction is the same as the geodetically determined extension direction (108°E, [24]), and comparable to that inferred from Quaternary dykes and open fissures within the magmatic segments (R. Gloaguen, personal communication, 2002). The timing of the change in extension direction within the northern

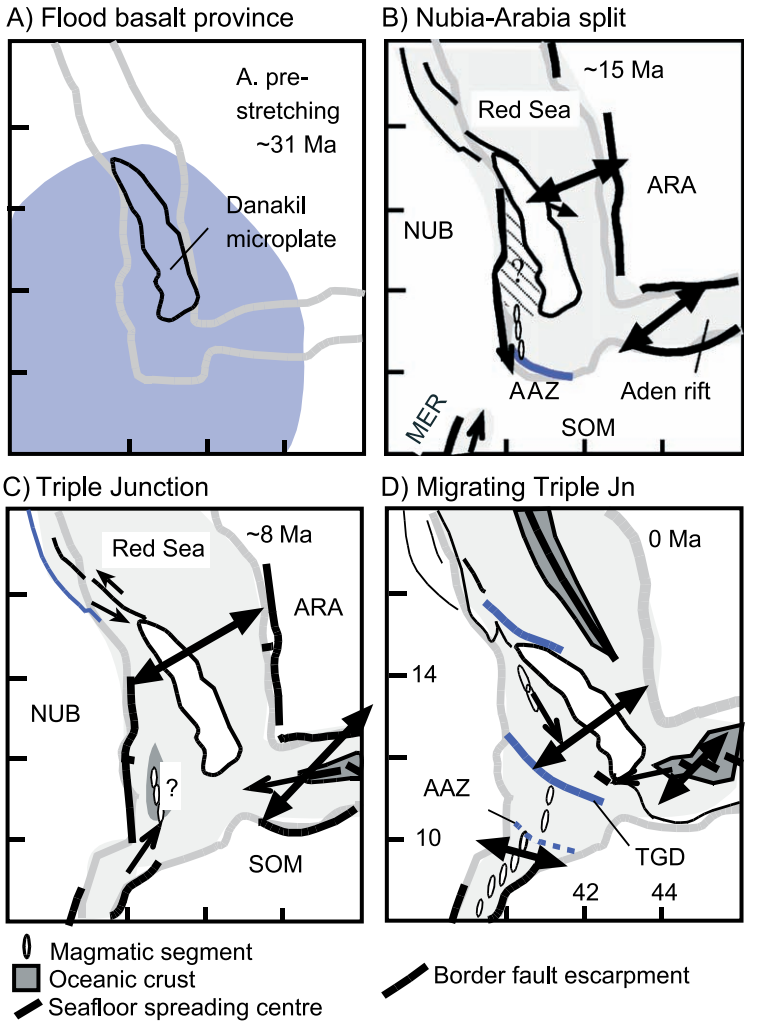

Fig. 9. Tectonic development of the Afar triple junction, illustrated with snapshots of representative stages. Relatively rigid blocks are shaded. Lighter stippling indicates regions which may have undergone small amounts of extension. Plate reconstructions from [6]. In all stages, arrows indicate along-axis propagation directions. (A) Between 35 and 27 Ma, continental rifting commences in Red Sea and Gulf of Aden. Arcuate accommodation zone (AAZ) of [5] marks previous location of southwestern Arabia. (B) By 15 Ma, rift basins in the southern Red Sea have accumulated several kilometers of volcano-sedimentary strata, and seafloor spreading has commenced in the eastern Aden rift. Extension between Nubia and Danakil microplate may have initiated. (C) After 11 Ma, extension in the Main Ethiopian rift propagates northward to form a triple junction for the first time. Greatest stretching has occurred in southern Afar, where some oceanic crust may have been created by 8 Ma. (D) Along-axis propagation of the Gulf of Aden and Red Sea spreading centres induced renewed extension and volcanism between 4 and 2 Ma. Magmatic segments form throughout the Main Ethiopian rift as it propagates northward to form the present-day triple junction.

MER is also consistent with predictions of Nubia–Somalia motions deduced from seafloor spreading anomaly patterns [41,42]. The middle Pliocene was a period of significant changes in plate boundaries and kinematics throughout the triple junction zone: seafloor spreading in the Red Sea commenced at ca. 4 Ma, concomitant with a massive outpouring of primarily basaltic lavas in Afar [20,43]. Eagles et al. [6] predict an increase in rate of opening in the Afar between 4–3 Ma. Thus, the change in extension direction may have been a response to along-axis propagation of seafloor spreading within the

Red Sea and Aden rifts, and adjustment to changing plate boundaries.

Geophysical and geomorphological data provide additional information on the zone of intersection of the Main Ethiopian and Red Sea rifts (e.g., Figs. 2 and 8). The Ankober border fault at the southern tip of the Red Sea rift lies on the opposite side of the rift from the Arboye border fault, and there is no evidence for structural linkage of these Mid-Miocene structures. Instead, patterns of faulting and seismicity show fault propagation and along-axis linkage within the central rift via a series of en echelon N10°E-striking faults linked by N35°E-striking ramps and transfer faults (Figs. 2 and 6). Epicentral locations of earthquakes recorded in 2002 and 2003 as well as historical records show clusters near the southern tip of the Ankober border fault, and along faults within and near the Quaternary magmatic segments [26]. Consistent kinks in stream drainage show that the <2.5 My Keradi fault system has propagated northeastward from the study region into the adjoining Baso-Werena basin, and southwestward toward the Boset magmatic segment [44]. Thus, independent data confirm the progressive localisation of strain and magmatism from the border fault systems to the central rift valley magmatic segments, as well as along-axis propagation of faulting.

7. Conclusions

New structural and stratigraphic observations and 10 new $^{40}Ar/^{39}Ar$ dates from the northern Main Ethiopian rift system reveal that initial extension commenced at $\sim$ 11 Ma when the NNE-trending Arboye border fault system developed. The Red Sea–Aden–Main Ethiopian rift triple junction is a relatively young feature; the northern Main Ethiopian rift developed $\sim$ 18 My after initial faulting in the southern Red Sea and western Gulf of Aden rifts. Integrating our new results with existing data, the Main Ethiopian rift, the northernmost sector of the East African rift system, propagated northward from the zone of superposed Mesozoic and Cenozoic rifting in the Turkana region after 25 Ma. Thus, the Main Ethiopian rift, which marks the incipient plate boundary between Nubia and Somalia, formed long after the flood basaltic magmatism, and not as a consequence of the separation of Arabia from Africa.

Between 6.6 and 3.5 Ma, extensional strain migrated from the border faults to smaller offset faults and aligned eruptive centres in the central rift valley. During this interval, which is marked by a widespread unconformity on the NW basin margin, normal fault orientations changed from predominantly N35°E to N10°E, possibly in response to changes in plate configuration within the Afar depression caused by along-axis propagation. By 1.8 Ma, strains and volcanism localised to $\sim$ 10-km-wide magmatic segments within the central rift, which are characterised by felsic volcanic constructs and mafic dyke-injection zones. Explosive volcanism characterises the entire 10.6 My rock record, with ignimbrites comprising roughly half the volume seen in outcrop.

Acknowledgements

Research was funded by National Geographic Grant 6998 and a Thomas Holloway scholarship awarded to EW. DA was supported by a travel grant from the Royal Society. We thank Bekele Abebe, Richard Gloaguen, Ashanafi Tesfaye, and Julie Rowland for the assistance during the field studies, and Laurent Jolivet, Tim Kusky, Norm Sleep, and Martin Menzies for the insightful reviews. ***[BW]***

Appendix A. Single-crystal laser fusion methodology

Two packages were prepared for irradiation; one that contained most of the analyzed sanidines and plagioclase, and a second that contained the basalt and sanidines E01-17 and E01-18. Material to be analyzed and standards were arranged in a ring configuration in small (ca. 2×2-mm pits) on an aluminium disk sample holder. These packages were irradiated for 20 and 5 h, respectively, at 1 MW in the Cd-lined, in-core CLICIT facility of the Oregon State University TRIGA reactor. The monitor mineral used was sanidine from the Fish Canyon Tuff of Colorado, with a reference age of 28.02 Ma [29].

Special care was taken to minimize the vertical neutron flux gradient affecting the sample package, and to statistically evaluate the lateral neutron flux

gradient. Over time, we have optimized the position of the sample packages in the reactor core to achieve the least vertical flux gradient. Measurement of standards in multi-level irradiations indicates that the vertical gradient is $<0.1\%$ over the 2.5–3-mm height of our Al disk sample holders. In addition, each of sample pits in the holder was filled to the top, and all material was analyzed—thus effectively averaging the remaining vertical gradient on a per-sample basis. The lateral flux gradient was measured using the monitor mineral interspersed along the ring with the samples (one standard for every two unknowns in a regularly repeating pattern). The various neutron parameter values (J's) obtained for the standards were regressed using a multi-variate planar fit using the known relative spatial coordinates of each pit. As is typical for irradiations in this reactor facility, the fit statistics for the first irradiation package indicated a very planar orientation for J's of the five standard positions ($R^2=0.989$, residuals $<0.06\%$). A conservative 1σ uncertainty of 0.1% was arbitrarily applied to the predicted J for the sample positions.

The standards and feldspar unknowns were fused with application of approximately 7 W of focused CO_2 laser energy under ultra-high vacuum, and analyzed for five argon isotopes using a MAP 215-50 mass spectrometer (see [30,31] for representative techniques). From 5 to 23 crystals were individually analyzed in the case of the feldspars. In the case of the basalt, about 20 mg was analyzed by the laser incremental-heating method using the CO_2 laser fitted with an integrator lens that produces a nominally flat, 6×6-mm beam profile.

References

[1] N. Hayward, C. Ebinger, Variations in along-axis segmentation of the Afar rift system, Tectonics 15 (1996) 244–257.

[2] I. Manighetti, P. Tapponnier, V. Courtillot, S. Gruszow, P.-Y. Gillot, Propagation of rifting along the Arabia–Somalia plate boundary: the gulfs of Aden and Tadjoura, J. Geophys. Res. 102 (1997) 2681.

[3] G. WoldeGabriel, T. White, G. Suwa, P. Renne, J. de Heinzelin, W. Hart, G. Heiken, Ecological and temporal placement of early Pliocene hominids at Aramis, Ethiopia, Nature 371 (1994) 330–333.

[4] D.P. McKenzie, D. Davies, P. Molnar, Plate tectonics of the Red Sea and East Africa, Nature 224 (1972) 125–133.

[5] S. Tesfaye, T.T. Kusky, D. Harding, Early Continental breakup boundary and migration of the Afar triple junction, Ethiopia, Geol. Soc. Amer. Bull. 115 (2003) 1053–1067.

[6] G. Eagles, R. Gloaguen, C. Ebinger, Kinematics of the Danakil microplate, Earth Planet. Sci. Lett. 203 (2002) 607–620.

[7] G. WoldeGabriel, J. Aronson, R. Walter, Geology, geochronology, and rift basin development in the central sector of the Main Ethiopian rift, Geol. Soc. Am. Bull. 102 (1990) 439–458.

[8] T. Chernet, W. Hart, J. Aronson, R.C. Walter, New age constraints on the timing of volcanism and tectonism in the northern Main Ethiopian Rift–southern Afar transition zone (Ethiopia), J. Volcanol. Geotherm. Res. 80 (1998) 267–280.

[9] J.-G. Schilling, R. Kingsley, B. Hanan, B. McCully, Nd–Sr–Pb isotopic variations along the Gulf of Aden: evidence for Afar mantle plume-continental lithosphere interaction, J. Geophys. Res. 97 (1992) 10927–10966.

[10] C. Ebinger, N. Sleep, Cenozoic magmatism throughout E Africa resulting from impact of a single plume, Nature 395 (1998) 788.

[11] C. Hofmann, V. Courtillot, G. Feraud, P. Rochette, G. Yirgu, E. Ketefo, R. Pik, Timing of the Ethiopian flood basalt event: implications for plume birth and global change, Nature 389 (1997) 838–841.

[12] J. Baker, L. Snee, M. Menzies, A brief Oligocene period of flood volcanism in Yemen, Earth Planet. Sci. Lett. 138 (1996) 39–55.

[13] I. Ukstins, P. Renne, E. Wolfenden, J. Baker, M. Menzies, Matching conjugate volcanic rifted margins: $^{40}Ar/^{39}Ar$ chrono-stratigraphy of pre- and syn-rift bimodal flood volcanism in Ethiopia and Yemen, Earth Planet. Sci. Lett. 198 (2002) 289–306.

[14] E. Wolfenden, C. Ebinger, G. Yirgu, P. Renne, S.P. Kelley, Evolution of the southern Red Sea rift: birth of a magmatic margin, Geol. Soc. Am. Bulletin (2004) in press.

[15] F. Watchorn, G. Nichols, D. Bosence, Rift-related sedimentation and stratigraphy, southern Yemen (Gulf of Aden), in: B. Purser, D. Bosence (Eds.), Sedimentation and Tectonics of Rift Basins, Chapman & Hall, London, 1998, pp. 165–189.

[16] C. Ebinger, T. Yemane, D. Harding, S. Tesfaye, D. Rex, S. Kelley, Rift deflection, migration, and propagation: linkage of the Ethiopian and Eastern rifts, Africa. Geol. Soc. Am. Bull. 102 (2000) 163–176.

[17] D'Acremont, E., De la déchirure continentale à l'accretion oceanique: Ouverture du Golfe d'Aden, thesis, Université de Paris VI, 2002, pp.

[18] J. Cochran, F. Martinez, Evidence from the northern Red Sea on the transition from continental to oceanic rifting, Tectonophysics 153 (1988) 25–53.

[19] G. Acton, A. Tessema, M. Jackson, R. Bilham, The tectonic and geomagnetic significance of paleomagnetic observations from volcanic rocks of central Afar, Earth Planet. Sci. Lett. 180 (2000) 225–241.

[20] T. Kidane, et al., New paleomagnetic results from Ethiopian Afar: determination of a ~2 Ma reference pole for stable Africa, J. Geophys. Res. 107 (2003) (10.1029/2001JB000645).

[21] I. Manighetti, P. Tapponnier, V. Courtillot, Y. Gallet, E. Jacques, P.-Y. Gillot, Strain transfer between disconnected, propagating rifts in Afar, J. Geophys. Res. 106 (2001) 13613–13665.
[22] B. Sichler, La bielette danakile: une modele pour l'evolution geodynamique de l'Afar, Bull. Soc. Geol. Fr. 22 (1980) 925–933.
[23] T. Souriot, J.-P. Brun, Faulting and block rotation in the Afar triangle, East Africa: the Danakil crank-arm model, Geology 20 (1992) 911–924.
[24] R. Bilham, R. Bendick, K. Larson, J. Braun, S. Tesfaye, P. Mohr, L. Asfaw, Secular and tidal strain across the Ethiopian rift, Geophys. Res. Lett. 27 (1999) 2789–2984.
[25] M. Boccaletti, R. Mazzuoli, M. Bonini, T. Trua, B. Abebe, Plio-Quaternary volcanotectonic activity in the northern sector of the Main Ethiopian rift: relationships with oblique rifting, J. Afr. Earth Sci. 29 (1999) 679–698.
[26] C.J. Ebinger, M. Casey, Continental breakup in magmatic provinces: an Ethiopian example, Geology 29 (2001) 527–530.
[27] P. Maguire, Geophysical project in Ethiopia studies continental breakup, Eos, Trans. Amer. Geophys. Union 84 (2003) 337–340.
[28] R. Mahatsente, G. Jentzsch, T. Jahr, Crustal structure of the Main Ethiopian rift from gravity data: 3-dimensional modelling, Tectonophysics 313 (1999) 363–382.
[29] P.R. Renne, C.C. Swisher III, A.L. Deino, D.B. Karner, T. Owens, D.J. DePaolo, Intercalibration of standards, absolute ages and uncertainties in $^{39}Ar/^{40}Ar$ dating, Chem. Geol. 145 (1998) 117–152.
[30] A.L. Deino, L. Tauxe, M. Monghan, R. Drake, $^{40}Ar/^{39}Ar$ age calibration of the litho and paleomagnetic stratigraphies of the Ngorora formation, Kenya, J. Geol. 98 (1990) 567–587.
[31] A.L. Deino, R. Potts, Single-crystal $^{40}Ar/^{39}Ar$ age calibration of the Olorgesailie Formation, Kenya. J. Geophys. Res. 95 (199) 8453–8470.
[32] S. Berhe, V. Kazmin, Nazret sheet NC37-15: Addis Ababa, Ethiopian Institute of Geological Surveys, scale 1:250,000 (1978).
[33] George, R. Thermal and tectonic controls on magmatism in the Ethiopian province, thesis, Open University, Milton Keynes, 1997, pp.
[34] P. Jones, Age of the lower flood basalts of the Ethiopian plateau, Nature 261 (1976) 567–569.
[35] W. Morton, D. Rex, J. Mitchell, P. Mohr, Riftward younging of volcanic units in the Addis Ababa region, Ethiopian rift valley, Nature 280 (1979) 284–288.
[36] L. Morbidelli, M. Nicoletti, C. Petrucciani, E. Piccirillo, Ethiopian southeastern plateau and related escarpment: K/Ar ages of the main volcanic events, in: A. Pilger, A. Rösler (Eds.), Afar Between Continental and Oceanic Rifting, Schweizerbart, Stuttgart, 1975, pp. 362–370.
[37] R. Pik, B. Marty, J. Carignan, J. Lave, Stability of the Upper Nile drainage network (Ethiopia) deduced from (U–Th)/He thermochronometry: implications for uplift and erosion of the Afar plume dome, Earth Planet. Sci. Lett. 215 (2003) 73–88.
[38] N. Bellahsen, C. Faccenna, F. Funiciello, J.M. Daniel, L. Jolivet, Why did Arabia separate from Africa? Insights from 3-D laboratory experiments, Earth Planet. Sci. Lett. 216 (2003) 365–381.
[39] C.K. Morley, W.A. Wescott, W.A. Stone, D.M. Harper, R.M. Wigger, F. Karanja, Tectonic evolution of the northern Kenya rift, J. Geol. Soc. (Lond.) 149 (1992) 333–348.
[40] R. Buck, L. Lavier, A.N.B. Poliakov, How to make a rift wide, Philos. Trans. R. Soc. Lond., A 357 (1999) 671–693.
[41] E. Calais, C. DeMets, J.-M. Nocquet, Evidence for post-3.16 Ma change in Nubia–Eurasia–North America plate motions, Earth Planet. Sci. Lett. 216 (2003) 81–92.
[42] J. Lemaux, R.G. Gordon, J.-Y. Royer, Location of the Nubia–Somalia boundary along the Southwest Indian Ridge, Geology 30 (2002) 339–342.
[43] B. Wolde, Spatial and temporal variations in the compositions of Upper Miocene to Recent basic lavas in the northern Main Ethiopian rift: implications for the causes of Cenozoic magmatism in Ethiopia, Geol. Rundsch. 85 (1996) 380–389.
[44] E. Wolfenden, Evolution of the Southern Red Sea Rift: Birth of a magmatic margin. Thesis, Royal Holloway, University of London, 2003, pp.
[45] T. McClusky, R. Reilinger, S. Mahmoud, D. Ben Sari, A. Tealeb, GPS constraints on Africa (Nubia) and Arabia plate motions, Geophys. J. Int. 155 (2003) 126–138.